# Epipolar Geometry for Vision-guided Laser Surgery

Nicolas Andreff, Sounkalo Dembélé, Brahim Tamadazte and Zill-e Hussnain
*Institut FEMTO-ST, Université de Franche-Comté/CNRS/ENSMM/UTBM, 24 rue Savary, 25000 Besançon, France*

Keywords: Laser Surgery, Visual Servoing, Epipolar Geometry.

Abstract: This paper proposes to use the analogy between a scanning laser beam and a camera. Thereby, a degenerate stereoscopic system can be defined by such a virtual camera and a real camera observing the laser spot on the tissues. This system can be mathematically described by means of epipolar geometry. From the latter, a vision-based control law which has no any matrix inversion nor estimation of the 3D scene is developed. According to the first results of simulation, the proposed control law shows an exponential convergence and robustness with the presence of noise in the sensors signals.

## 1 INTRODUCTION

$\mu$RALP is an European FP7-ICT project that involves the development of a system for endoluminal laser phonosurgery, *i.e.* surgery of the vocal chords using an incision laser emitted from fiber optics inside the larynx (Fig. 2). Unlike $\mu$RALP project, in current laryngeal laser surgical procedures, a beam of incision laser is projected to target position on the soft tissue, from the working distance of 400mm by means of a rigid laryngoscope (Fig. 1). This yields safety concerns for the patient and staff due to the fact that laser beam follows an uncovered path toward surgical site as shown in the Fig. 1, as well as limitations to accuracy, since a large working distance limits the minimum accuracy achieved by a typical laser scanner. Moreover, this so-called *laryngeal suspension* posture of the patient requires an extreme stretching of the neck, which makes current surgical procedure painful even several days after the operation.

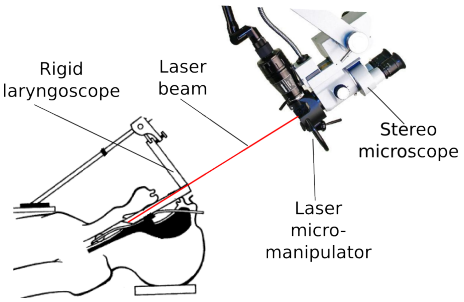


Figure 1: Current laryngeal laser surgery setup.

One such laryngeal laser surgical system is the AcuBlade™. It claims to be a robotic system because it features fully autonomous pattern following (line and arc for resection, circle for ablation) by the laser spot, once the surgeon has defined the dimension and the position of the pattern intraoperatively based on direct visualization (through the stereomicroscope) of the operating site. Thus, the laser spot is automatically controlled. So by competitive rationalism the objective of $\mu$RALP is also to automate the control of the laser phonosurgery, which is totally in line with the industrial and medical practices in the field.

Yet, in the AcuBlade system, the laser spot is controlled in an open-loop mode from the surgeon's viewpoint. Once the surgeon has chosen the pattern parameters, the robot follows it blindly, relying on its internal calibration and sensors. Any deviation from this plan is forbidden (to the exception of the foot pedal switch of the power laser). The movement of the target tissue during surgery can bring incorrect target position under projected laser beam, and when surgeon realizes, it may be too late to switch off the incision laser using foot pedal. Indeed, during the ablation and the resection, the tissue moves(by breathing or heart beat) and deforms (due to resection). Therefore, the planned pattern must be very small and cannot guarantee high accuracy. Furthermore, in case of an endoscopic laser steering system (Fig. 2), one cannot guarantee any time stability of the microrobot calibration.

The only way to increase the accuracy and the extension of the patterns is to close the control loop over an exteroceptive sensor, namely the imaging system. Closing the control loop over a camera is known as

Andreff N., Dembélé S., Tamadazte B. and Hussnain Z..
Epipolar Geometry for Vision-guided Laser Surgery.
DOI: 10.5220/0004595904710476
In *Proceedings of the 10th International Conference on Informatics in Control, Automation and Robotics* (ICINCO-2013), pages 471-476
ISBN: 978-989-8565-71-6

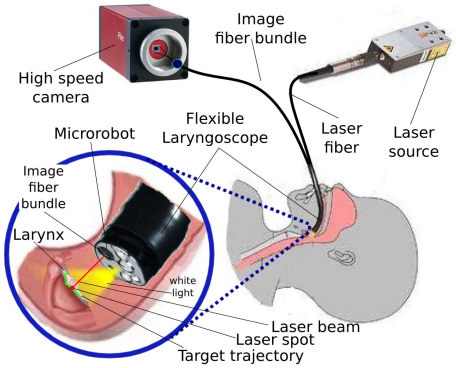


Figure 2: Endoscopic laser microphonosurgery.

visual servoing, known as being a technique robust to calibration errors and dynamics of hand-and-eye coordination.

Visual servoing has been used in minimally invasive surgery to perform two types of applications. The first type is relative to tissue motion tracking and compensation. By opposition to industrial objects, human tissues are alive and have tendency to move by breathing or beating heart motions. These physiological motions complicate the task of the surgeon, and their compensation improves the precision of surgical interventions. The second type of applications deals with tracking and guidance of surgical instruments. In this case, the objective is more classical for visual servoing: positioning of a target by using vision-based feedback control.

## 1.1 Motion Compensation

In motion compensation using image-based control strategy, the motion of issue is estimated from images delivered by the vision system and compensated by means of a robotized instrument. Gangloff and his colleagues have developed an active beating heart stabilizer by using a predictive control scheme (Ginhoux et al., 2005) and a robust control scheme (Bachta et al., 2011). They obtained interesting results with simulation experiments as well as in-vivo experimental tests with pigs. In both cases the acquisition rate reached 500 Hz. In (Krupa et al., 2009), the authors used visual servoing and speckle information in ultrasound images at 12 Hz to stabilize a probe in a region of interest. Simulation experiments have been used to validate the developments. In (Kesner et al., 2010), the authors integrated heart motion compensation in the 3D positioning of a catheter using 3D ultrasound images. A Kalman filtering has allowed to take into account the 50-100 ms delay of acquisition and a tracking error of 0.77 mm was obtained with in-vivo tests with pigs. In (Chen et al., 2010) a virtual bone clamper is achieved by means of visual servoing with a stereovision system running at 10 Hz associated to a Kalman filtering. The core of these applications is motion tracking and for that solutions already developed in machine vision can be used: correlation (Ortmaier et al., 2005), Lucas-Kanade tracker or SURF (Elhawary and Popovic, 2011).

## 1.2 Instrument Guidance

In instrument guidance by means of visual servoing many developments have been reported in the literature. In 2003, Krupa et *al.* (Krupa et al., 2003) proposed the use of image-based visual servoing to perform 3D positioning of a surgical instrument. But only simulation experiments were performed with a camera running at 50 Hz and a phantom instrument. The same group proposed the 3D positioning of a probe using visual servoing in ultrasound images: image-based visual servoing on a simulation set-up in (Krupa and Chaumette, 2006), visual servoing using moments on simulation set-up running at 25 Hz (Mebarki et al., 2010). In (Becker et al., 2010), the authors have developed a semi-automated laser intraocular surgery. Their set-up included a laser probe attached to a micromanipulator, a stereovision system working at 30 Hz, a 3D sensor running at 2 kHz and a control system running at 1 kHz. All the application aspects were presented: preoperative procedure for the selection of the sites to burn, calibration of stereovision device using the data of the 3D sensor, 3D surface reconstruction and registration of current images with preoperative images, PID control of the micromanipulator to position the laser on the site to burn. Note that the control is a PID in the 3D space over the triangulated laser spot.

In (Mattos and Caldwell, 2012) and (Dagnino et al., 2012), Mattos describes their experiments in laser phonomicrosurgery. They have integrated complete equipment including laser sources, micromanipulators to control the position of the laser beam, an optical microscope to view and record the images and a haptic device. They also developed different algorithms to track the laser spot following a predefined path. For the moment, these works treat the problem in a static point of view, thus the dynamics aspects of the systems (3D tissue, tissue movement, kinematic model of microrobot, etc.), were not included in the study. In (Reilink et al., 2010), the authors used directly images delivered by an endoscope to guide it inside the body. Simulation experiment show an improvement of 68% with respect to manual steering.

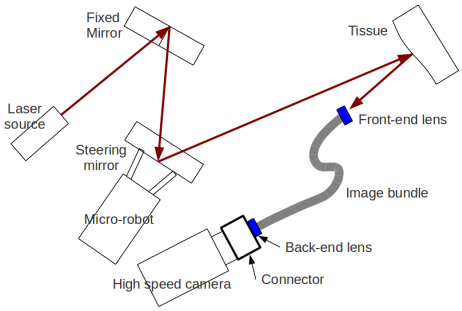


Figure 3: Schematic view of the laser steering system.

### 1.3 Related Developments

In addition to the literature above dealing with visual servoing directly, it is also necessary to cite the references (Ota et al., 2009; Rivera-Serrano et al., 2012) which describe the development of a flexible robot for transoral surgery. It is a snake-like mechanism of 10 mm diameter, 300 mm long including 105 degrees-of-freedom. It is endowed with a 15 K fiber bundle connected to a 640×480 pixels camera, an illumination source, and two 4.2 mm tool ports. It has been possible to introduce it in cadavers without laryngeal suspension, to observe vocal folds and to perform a retraction and cauterization on the base of the tongue. However, the system is only working in teleoperated mode which might limit its accuracy with respect to the delicate phonosurgery requirements. Such a system should thus be enhanced by adding visual servoing and, probably also, a laser by replacing the currently used mechanical scalpel.

### 1.4 Contributions

The contribution of this paper is to discuss the control of a laser (namely, the invisible incision laser for incision with co-axial visible red color Helium–Neon laser pointer) over the vocal folds, and by extension, the control of a laser over any surface. It shows that the geometrical relation between laser scanner and camera can simplify the control of microrobot (for laser scanner): no matrix inversion, no explicit knowledge or reconstruction of the 3D scene.

## 2 VISUALLY-GUIDED LASER SURGERY

In this section, we analyze the control of the laser spot with the microrobot using an optic fiber bundle to bring the image of the scene onto a high-speed camera (see Fig. 2 and Fig. 3).

This control can be done in two ways: using the standard visual servoing equations or using the above grounding analogy.

### 2.1 A Word on Standard Control

Let us note ${}^0\underline{z}$ the direction of the laser beam reflecting from the steering mirror towards the vocal fold, $P$ the position of the laser spot on the tissue surface, and $p$ the position of the laser spot in the image. Then, it is trivial to write, in the reference frame $R_0$, attached to the zero-reference of the steering mirror, the following equation:

$$ {}^0P = d\,{}^0\underline{z} \tag{1}$$

where $d$ is the distance traveled by the laser from the mirror to the tissue.

This distance cannot be measured, to the contrary of ${}^0\underline{z}$ which can be obtained from the microrobot encoders. However, it can be modeled if one approximates the tissue surface in $P$ by a plane equation:

$$ {}^0\underline{n}^T\,{}^0P - d_0 = 0 \tag{2}$$

where ${}^0\underline{n}$ is the orientation of the surface normal in $R_0$ and $d_0$ is the distance of the plane to the origin of $R_0$. Using this model, one finds:

$$ d = \frac{d_0}{{}^0\underline{n}^T\,{}^0\underline{z}} \tag{3}$$

On the other hand, the perspective projection equation yields:

$$ \tilde{p} = \mathbf{K}\frac{{}^cP}{Z} \tag{4}$$

where $\mathbf{K}$ is the matrix containing the camera intrinsic parameters, $P$ is now expressed in the camera frame $R_c$, $Z$ is the unmeasured depth along the line of sight passing through $p$ as well as the third coordinate of ${}^cP$ and $\tilde{p}$ represents the homogeneous coordinates of $p$.

To apply, the usual visual servoing approach, one needs to differentiate the latter with time (ie. time-derivation):

$$ \dot{\tilde{p}} = \frac{1}{Z}\mathbf{K}\begin{pmatrix} 1 & 0 & -X/Z \\ 0 & 1 & -Y/Z \\ 0 & 0 & 0 \end{pmatrix} {}^c\dot{P} \tag{5}$$

where $X$, $Y$, and $Z$ are the 3D coordinates of ${}^cP$.

It is possible to obtain another expression of ${}^c\dot{P}$ by differentiating (1):

$$ {}^0\dot{P} = \dot{d}\,{}^0\underline{z} + d\,{}^0\dot{\underline{z}} \tag{6}$$

and expressing the latter in $R_c$:

$$ {}^c\dot{P} = {}^c\mathbf{R}_0\left(\dot{d}\,{}^0\underline{z} + d\,{}^0\dot{\underline{z}}\right) \tag{7}$$

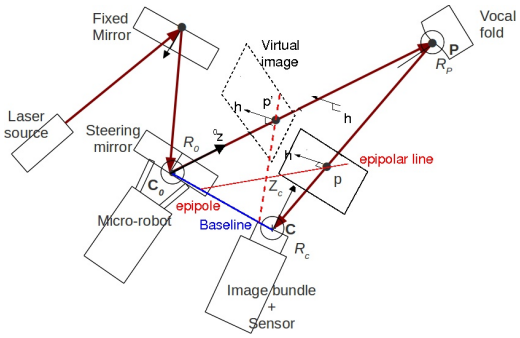


Figure 4: Analogy with stereoscopy.

Now, from (3), one gets (under the simplifying assumption that the surface plane does not change):

$$\dot{d} = -\frac{d_0 {}^0\underline{n}^T}{({}^0\underline{n}^T {}^0\underline{z})^2} {}^0\dot{\underline{z}} \tag{8}$$

Putting (7) and (8) into (5) allows to obtain $\dot{\tilde{p}}$ under the following form:

$$\dot{\tilde{p}} = \mathbf{L}(d, Z, {}^0\underline{n}, d_0, {}^c\mathbf{R}_0, p, {}^0\underline{z}) {}^0\dot{\underline{z}} \tag{9}$$

where $\mathbf{L}$ is of dimension $3 \times 3$. The inversion of the latter allows to convert the image velocity of the laser spot into the velocity of the laser beam, which, in turn, shall be converted into microrobot velocity through the differential inverse kinematic model.

Therefore, this controller needs the estimation of $d$ and $Z$, which can be obtained by triangulation between the laser beam (known from the joint values $q$), the line of sight outgoing from the camera through the laser spot projection ($p$) and the robot-camera calibration.

We have not implemented this controller, nor pushed further the details of the calculation (so far), because there is a more elegant way of treating the problem, which does not require any explicit triangulation nor matrix inversion.

## 2.2 Laser Visual Servoing using Epipolar Geometry

On the opposite to the above method, which is totally generic, our approach, detailed, below is totally handmade and tailored to the specific case of a laser beam being observed by a camera.

Indeed, the set-up in Fig. 3 is analogous to a degenerate case of epipolar geometry in Fig. 4: the steering mirror is similar to a virtual camera whose optical centre corresponds to the centre of rotation of the mirror. Thereby, points $p$ and $p'$ are the images of the same spatial point $P$ and are hence linked by the epipolar constraint:

$$\tilde{p}'^{\top} \mathbf{F} \tilde{p} = 0 \tag{10}$$

where $\mathbf{F}$ is the fundamental matrix of the two-view system (Hartley and Zisserman, 2006). Actually, this epipolar constraint is defined up to a scale factor, and thereby, $\tilde{p}'$ can be replaced by ${}^0\underline{z}$, the unit vector describing, in the microrobot base-frame $R_0$, the direction of the laser beam from the mirror to the vocal fold:

$${}^0\underline{z}^{\top} \mathbf{F} \tilde{p} = 0 \tag{11}$$

This equation expresses the fact that the origin of the camera, the pivot point of the microrobot, the laser beam, the line of sight and the laser spot on the tissue are coplanar. It can be also interpreted in three ways:

$${}^0\underline{z} \perp \mathbf{F}\tilde{p} \tag{12}$$

$$\tilde{p} \perp \mathbf{F}^{\top} {}^0\underline{z} \tag{13}$$

and both $\mathbf{F}\tilde{p}$ and $\mathbf{F}^{\top} {}^0\underline{z}$ represent the (non-unit) normal vector to the epipolar plane in the micro-robot and the camera frame, respectively.

The time derivative of the epipolar constraint which is given by:

$$(\mathbf{F}^{\top} {}^0\underline{z})^{\top} \dot{\tilde{p}} + (\mathbf{F}\tilde{p})^{\top} {}^0\dot{\underline{z}} = 0 \tag{14}$$

Now, we can decompose ${}^0\dot{\underline{z}}$ into a component orthogonal to the epipolar plane and a component inside the latter:

$${}^0\dot{\underline{z}} = \alpha {}^0\underline{h} + \beta {}^0\underline{z} \times {}^0\underline{h} \tag{15}$$

where ${}^0\underline{h} = \frac{\mathbf{F}\tilde{p}}{\|\mathbf{F}\tilde{p}\|}$. Replacing this expression into the epipolar constraint and reordering the terms, we get:

$$\alpha = -\frac{(\mathbf{F}^{\top} {}^0\underline{z})^{\top}}{\|\mathbf{F}\tilde{p}\|} \dot{\tilde{p}} \tag{16}$$

Actually, $\alpha$ only depends on the projection of $\dot{\tilde{p}}$ onto the normal to the epipolar plane, but expressed in the camera frame, *i.e.* along ${}^c\underline{h} = \frac{\mathbf{F}^{\top} {}^0\underline{z}}{\|\mathbf{F}^{\top} {}^0\underline{z}\|}$. Thus, the remaining part of $\dot{\tilde{p}}$ is obtained by canceling this projection:

$$\dot{\tilde{p}} = a {}^c\underline{h} + (\mathbf{I}_3 - {}^c\underline{h} {}^c\underline{h}^{\top}) \dot{\tilde{p}} \tag{17}$$

where the value of $a$ does not have any interest for the sequel, but can be related to $\alpha$ by inserting the latter equation into the former.

Now, concentrate on the part of $\dot{\tilde{p}}$ lying in the epipolar plane. In (17), it is expressed in the camera frame, so we just need to bring it back to the microrobot frame, going backwards the camera intrinsic parameters, the orientation of the camera frame with respect to the microrobot frame and compensating for the unknown scale factor in $\mathbf{F}$, to get $\beta$:

$$\beta = \frac{\|\mathbf{F}^{\top} {}^0\underline{z}\|}{\|\mathbf{F}\tilde{p}\|} ({}^0\underline{z} \times {}^0\underline{h})^{\top} {}^0\mathbf{R}_c \mathbf{K}^{-1} (\mathbf{I}_3 - {}^c\underline{h} {}^c\underline{h}^{\top}) \dot{\tilde{p}} \tag{18}$$

As a consequence, we have expressed ${}^0\dot{\underline{z}}$ as a function of $\dot{\tilde{p}}$:

$$ {}^0\dot{\underline{z}} = \left\{ ({}^0\underline{z} \times {}^0\underline{h})({}^0\underline{z} \times {}^0\underline{h})^\top {}^0\mathbf{R}_c \mathbf{K}^{-1} (\mathbf{I}_3 - {}^c\underline{h}\,{}^c\underline{h}^\top) - {}^0\underline{h}\,{}^c\underline{h}^\top \right\} \frac{\|\mathbf{F}^\top {}^0\underline{z}\|}{\|\mathbf{F}\tilde{p}\|} \dot{\tilde{p}} \quad (19) $$

Consequently, we have the exact expression of the conversion of the image velocity into the laser beam velocity, without any matrix inversion, nor any explicit triangulation or scene structure knowledge. This expression only depends on the measurements (${}^0\underline{z}$ and $p$), the fundamental matrix $\mathbf{F}$ and a reduced set of calibration parameters ($\mathbf{K}$ and ${}^c\mathbf{R}_0$). Geometry is always useful !

Now, we can come up to the control law, by enforcing a first order behavior of the error in the image between the current and the desired projections of the laser spot in the image:

$$ \dot{\tilde{p}} = -\lambda(\tilde{p} - \tilde{p}^*) \quad (20) $$

with $\tilde{p}^*$ the set point and $\lambda$ the control gain.

The joint space control of the microrobot is given by:

$$ \dot{q} = \mathbf{J}^{-1}\, {}^0\dot{\underline{z}} \quad (21) $$

where $\mathbf{J}^{-1}$ is the inverse kinematic Jacobien of the microrobot.

## 3 SIMULATION RESULTS

The experimental validation of the proposed approach consists of a simulator before a real implementation on an experimental setup. The used simulator was implemented using the Open Source C++ Library: ViSP (Visual Servoing Platform) (Marchand et al., 2005). So, in first case, we have studied the convergence of the proposed control law in perfect conditions (no noise). Figure 5 illustrates the expected exponential decay of the image errors on both microrobot's degrees-of-freedom *vs.* the time variation.

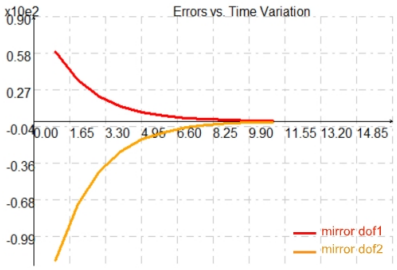


Figure 5: Time evolution of the image errors.

In order to test the robustness of the proposed control law, we have added Gaussian white noise to the sensors signals ($\tilde{p}^*$ and ${}^0\underline{z}$). Therefore, Figure 6 shows that the control law remains efficient and converges exponentially to zero despite the presence of noise on the measurements.

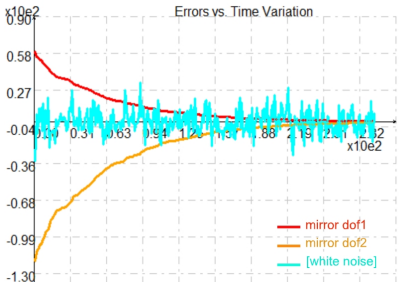


Figure 6: Time evolution of the image errors with error measurements (*ie.* with added noise).

## 4 DISCUSSION

Under real conditions of endoscopic phonomicrosurgery using a laser, the surgeon sets a 3D path onto the vocal cords to be followed by the laser with a high accuracy. However, the proposed approach does not include the trajectory tracking in the mathematical formulation of the control law. Therefore, it should be complemented by an additional term for trajectory tracking purpose ($\tilde{p}^*(t)$), including constraints on the tissue exposure to laser, in order to avoid any carbonization. Further investigation of geometry, namely the trifocal geometry associated to a stereoscopic observation of the laser spot, is expected to further simplify the control and to increase its robustness, which is a key issue in the transfer of automation into actual clinical devices. Also, many micromanipulators have a parallel kinematics architecture, which can be controlled without having joint encoder values as feedback (Andreff and Martinet, 2009). Consequently, using the proposed multi-view geometric approach might enable simplified miniaturization of laser steering in an endoscopic set-up, because one can design steering parallel kinematics mechanisms without proprioceptive sensors. This is a very crucial investigation field, since endoscopic laser surgery faces very contradictory requirements in terms of sweeping range and frequency (yielding larger mechanisms) and of available space at the endoscopic tip.

## 5 CONCLUSIONS

In this paper, it was shown that resorting to geometry simplifies the eye-to-hand control law for a surgical

laser (and any other application where a beam needs be accurately swept over a surface), by essentially removing the need for on-line estimation of the 3D surface. Actually, if a dedicated surgeon-robot interface is designed (Mattos and Caldwell, 2012) to define the desired trajectory in the image, then the latter will geometrically contain a coherent description of the 3D surface. And thus, the 3D information is not purely and simply thrown away as it could seem but, rather, it is implicitly used. The first obtained results of the simulation validation shows the relevance of the proposed approach. It provides a good convergence (exponential decay of the errors image) and robustness with respect to the presence of noise in the sensor signals. In the future, we will work on demonstrating the stability of the visual servoing control law and its validation on a testbench which includes a camera, a commercial laser and a micromirror equipped with a two degree-of-freedom scanner from PI (Physical Instruments Inc.). This is before considering validation tests on anatomical specimens

## ACKNOWLEDGEMENTS

This work was supported by $\mu$RALP, the EC FP7 ICT Collaborative Project no. 288663 (`http://www.microralp.eu`), and by ACTION, the French ANR Labex no. "ANR-11-LABX-01-01" (`http://www.labex-action.fr`).

## REFERENCES

Andreff, N. and Martinet, P. (2009). Vision-based self-calibration and control of parallel kinematic mechanisms without proprioceptive sensing. *Intelligent Service Robotics*, 2(2):71–80.

Bachta, W., Renaud, P., Laroche, E., Forgione, A., and Gangloff, J. (2011). Active stabilization for robotized beating heart surgery. *IEEE Transactions on Robotics*, 27:757–568.

Becker, B. C., MacLachlan, R. A., Jr, L. A. L., and Riviere, C. N. (2010). Semiautomated intraocular laser surgery using handheld instruments. *Lasers in Surgery and Medicine*, 42:264?273.

Chen, C.-S., Hsieh, M.-S., Chiu, Y.-W., Tsai, C.-H., Liu, S.-M., Lu, C.-C., and Yen, P.-L. (2010). An unconstrained virtual bone clamper for knee surgical robot using visual servoing technique. *Journal of the Chinese Institute of Engineers*, 33(3):379–386.

Dagnino, G., Mattos, L. S., and Caldwell, D. G. (2012). New software tools for enhanced precision in robot-assisted laser phonomicrosurgery. In *34th Annual International Conference of the Engineering in Medicine and Biology Society (EMBC'12)*.

Elhawary, H. and Popovic, A. (2011). Robust feature tracking on the beating heart for a robotic-guided endoscope. *The international journal of medical robotics and computer assisted surgery*, 7:459–468.

Ginhoux, R., Gangloff, J., de Mathelin, M., Soler, L., Sanchez, M. M. A., and Marescaux, J. (2005). Active filtering of physiological motion in robotized surgery using predictive control. *IEEE Transactions on Robotics and Automation*, 21(1):235–246.

Hartley, R. and Zisserman, A. (2006). *Multiple view geometry in computer vision*. Cambridge University Press, Cambridge, United Kingdom, 2nd edition edition.

Kesner, S. B., Yuen, S. G., and Howe, R. D. (2010). Ultrasound servoing of catheters for beating heart valve repair. In *IPCAI*, pages 168–178.

Krupa, A. and Chaumette, F. (2006). Guidance of an ultrasound probe by visual servoing. *Advanced Robotics*, 20(11):1203–1218.

Krupa, A., Fichtinger, G., and Hager, G. D. (2009). Real-time motion stabilization with b-mode ultrasound using image speckle information and visual servoing. *International Journal of Robotics Research*.

Krupa, A., Gangloff, J., Doignon, C., de Mathelin, M. F., Morel, G., Leroy, J., Soler, L., and Marescaux, J. (2003). Autonomous 3-d positioning of surgical instruments in robotized laparoscopic surgery using visual servoing. *IEEE Transaction on Robotics and Automation*, 19:842–853.

Marchand, E., Spindler, F., and Chaumette, F. (2005). Visp for visual servoing: a generic software platform with a wide class of robot control skills. *IEEE Robotics and Automation Magazine*, 12(4):40–52.

Mattos, L. S. and Caldwell, D. G. (2012). Safe teleoperation based on flexible intraoperative planning for robot-assisted laser microsurgery. In *34th Annual International Conference of the Engineering in Medicine and Biology Society (EMBC'12)*.

Mebarki, R., Krupa, A., and Chaumette, F. (2010). 2-d ultrasound probe complete guidance by visual servoing using image moments. *IEEE Transactions on Robotics*, 26(2):296–306.

Ortmaier, T., Groger, M., Boehm, D., Falk, V., and Hirzinger, G. (2005). Motion estimation in beating heart surgery. *IEEE Transactions on Biomedical Engineering*, 52(10):1729–1740.

Ota, T., Degani, A., Schwartzman, D., Zubiate, B., McGarvey, J., Choset, H., and Zenati, M. A. (2009). A highly articulated robotic surgical system for minimally invasive surgery. *The Annals of Thoracic Surgery*, 87(4):1253–1256.

Reilink, R., Stramigioli, S., and Misra, S. (2010). Image-based flexible endoscope steering. In *The 2010 IEEE/RSJ International Conference on Intelligent Robots and Systems*, pages 2339–2344.

Rivera-Serrano, C. M., Johnson, P., Zubiate, B., Kuenzler, R., Choset, H., Zenati, M., Tully, S., and Duvvuri, U. (2012). A transoral highly flexible robot: Novel technology and application. *The Laryngoscope*, 122:1067–1071.